OXFORD

ORIGINAL ARTICLE

# Tumor-on-a-chip platform to interrogate the role of macrophages in tumor progression

Ye Bi[1], Venktesh S. Shirure[2], Ruiyang Liu[3,4], Cassandra Cunningham[1], Li Ding[3,4], J. Mark Meacham[5], S. Peter Goedegebuure[1,6], Steven C. George[2,†], and Ryan C. Fields[1,6,*,†]

[1]Department of Surgery, Washington University School of Medicine, St. Louis, MO 63110, USA, [2]Department of Biomedical Engineering, University of California Davis, Davis, CA 95616, USA, [3]Department of Medicine, Washington University in St. Louis, St. Louis, MO 63110, USA, [4]McDonnell Genome Institute, Washington University in St. Louis, St. Louis, MO 63108, USA, [5]Department of Mechanical Engineering & Materials Science, Washington University in St. Louis, St. Louis, MO 63130, USA, and [6]Siteman Cancer Center, Washington University School of Medicine, St. Louis, MO 63110, USA

*Corresponding author. E-mail: rcfields@wustl.edu
†Authors contributed equally

## Abstract

Tumor-infiltrating leukocytes, in particular macrophages, play an important role in tumor behavior and clinical outcome. The spectrum of macrophage subtypes ranges from antitumor 'M1'-type to protumor 'M2'-type macrophages. Tumor-associated macrophages (TAMs) typically display phenotypic features of both M1 and M2, and the population distribution is thought to be dynamic and evolves as the tumor progresses. However, our understanding of how TAMs impact the tumor microenvironment remains limited by the lack of appropriate 3D *in vitro* models that can capture cell–cell dynamics at high spatial and temporal resolution. Using our recently developed microphysiological 'tumor-on-a-chip' (TOC) device, we present here our findings on the impact of defined macrophage subsets on tumor behavior. The TOC device design contains three adjacent and connected chambers in which both the upper and lower chambers are loaded with tumor cells, whereas the central chamber contains a dynamic, perfused, living microvascular network. Introduction of human pancreatic or colorectal cancer cells together with M1-polarized macrophages significantly inhibited tumor growth and tumor-induced angiogenesis. Protein analysis and antibody-based neutralization studies confirmed that these effects were mediated through production of C-X-C motif chemokines (CXCL9), CXCL10 and CXCL11. By contrast, M2-macrophages mediated increased tumor cell migration into the vascularized chamber and did not inhibit tumor growth or angiogenesis. In fact, single-cell RNA sequencing showed that M2 macrophages further segregated endothelial cells into two distinct subsets, corresponding to static cells in vessels versus active cells involved in angiogenesis. The impact of M2 macrophages was mediated mostly by production of matrix metalloproteinase 7 and angiopoietin 2. In summary, our data demonstrate the utility of the TOC device to mechanistically probe biological questions in a 3D *in vitro* microenvironment.

**Key words:**  tumor-on-a-chip; macrophage; angiogenesis; tumor invasion

**INSIGHT BOX**

Macrophages in the tumor microenvironment are key determinants of tumor behavior and clinical outcome. The macrophage subset composition and its functional impact change as tumors progress or during treatment, but adequate models to study this are lacking. We developed a tumor-on-a-chip model of perfused 3D tumor growth to probe the impact of defined macrophage subsets on features such as tumor migration and angiogenesis. Our data are consistent with previously described macrophage activity in the tumor microenvironment and provides potential new molecular targets. Herein, we demonstrate feasibility of probing immune–oncology questions in a 3D *in vitro* microenvironment.

## INTRODUCTION

Inflammatory cells, such as macrophages, play a central role in tumor progression, including tumor cell proliferation, angiogenesis as well as other central processes that shape the tumor microenvironment. Macrophages are particularly interesting as ample evidence has demonstrated a range of phenotypes that can either enhance or inhibit tumor progression depending on the macrophage polarization state [1–4]. While classification of macrophages is ongoing, an instructive categorization has been the so-called 'M1' and 'M2' designations [5, 6]. The former generally refers to macrophages that participate in cell killing, and thus can limit tumor progression, whereas the latter facilitates normal processes such as wound healing and tissue growth and can aid in tumor progression. Understanding the mechanisms that dictate trafficking and differentiation of the macrophage subtypes has generally been limited to 2D cell culture and animal models, both of which have severe limitations. For example, simply plating primary monocytes on a 2D surface initiates differentiation into macrophages, while animal models have limited spatial and temporal resolution to tease apart mechanisms that influence cell trafficking.

We recently reported the design of a microphysiological 'tumor-on-a-chip' (TOC) device [7] to study cancer biology. The device design contains multiple adjacent chambers that can be loaded with 3D tissue mimics at different points in time providing tremendous flexibility in the type of tissue and the question(s) that might be addressed. A central feature of the device is a dynamic, perfused, living microvascular network that is ideally suited to examine questions related to angiogenesis in settings such as the tumor microenvironment.

Our current study endeavored to use this device platform to demonstrate its utility to probe questions related to the impact of immune cells (macrophages) on tumor behavior and specifically interrogate the mechanisms by which macrophages in the tumor microenvironment can modulate tumor cell proliferation and migration, as well as angiogenesis—an important hallmark of cancer [8]. Our results demonstrate that macrophages survive, proliferate and traffic within the microfluidic device. Furthermore, using a range of biological techniques including single-cell RNA sequencing (scRNA-seq), as well as both colorectal cancer (CRC) and pancreatic ductal adenocarcinoma (PDAC) patient-derived cell lines, we discovered that the M1 macrophage inhibited angiogenesis and tumor cell growth through the enhanced production of a series of C-X-C motif chemokines (CXCL9, CXCL10 and CXCL11). In contrast, the M2 macrophage stimulated tumor cell migration through the enhanced secretion of a series of proteins that included matrix metalloproteinase 7 (MMP7) and angiopoietin 2 (ANGPT2). These results align with previous reports in the literature regarding the roles of CXCL9, CXCL10 and ANGPT2 [9–12] and also provide new potential targets (e.g. CXCL11 and MMP7) to

limit tumor progression [13, 14]. Further, they demonstrate the utility of the device to probe biological questions in a 3D *in vitro* microenvironment mechanistically.

## MATERIAL AND METHODS

### Cell lines and reagents

Normal human lung fibroblasts (NHLFs) were obtained from Lonza (Basel, Switzerland), and endothelial colony-forming cell-derived endothelial cells (ECFC-ECs) were extracted from cord blood as detailed previously [15]. Both cell types were cultured and used in TOC devices for up to seven passages in complete growth medium from Lonza (Fibroblast Growth Medium-2 (FGM-2) for NHLFs and Endothelial Growth Medium-2 (EGM-2) for ECFC-ECs). The CRC cell lines (CRC268, CRC663, CRC1180) and PDAC cell lines (PDAC162, PDAC175) were generated *in vitro* from low passage number patient-derived xenografts established in NOD-SCID mice by the Solid Tumor Tissue Bank and Registry at the Washington University in St. Louis. All tumor cell lines were cultured using RPMI1640 medium with 10% fetal bovine serum and antibiotics. Monocyte cell lines THP-1 (ATCC® TIB-202™) and U-937(ATCC® CRL-1593.2™), and CRC tumor lines SW480 and SW620 as well as PDAC lines HPAC and Panc1 were obtained from ATCC and cultured in the recommended medium. Reagents used in the *in vitro* macrophage differentiation were as below: phorbol 12-myristate 13-acetate (PMA) and lipopolysaccharides (LPS) were obtained from Sigma-Aldrich (Darmstadt, Germany). Recombinant human interleukin-4 (IL-4), interleukin-13 (IL-13) and interferon-gamma (IFN-$\gamma$) were purchased from PeproTech (Rocky Hill, NJ).

### Cell transduction

The ECFC-ECs were transduced with a green fluorescent protein (GFP)-expressing lentivirus to constitutively express GFP as detailed previously [15]. Colorectal and pancreatic cancer cell lines were transduced using red fluorescent protein (RFP) and puromycin-encoding lentiviral particles obtained from GenTarget Inc. (San Diego, CA) following the recommended protocol. Briefly, cancer cells were seeded into 24-well tissue culture plates and incubated overnight at 37°C in 5% $CO_2$. The next day, the medium was replaced with 0.5 ml of complete culture medium and 50 μl of lentivirus particles. In total, 72 hours after transduction, the medium was replaced with 1 ml complete medium containing 1 μg/ml puromycin for selection to generate stable cell lines expressing RFP.

### Device manufacture, device loading and tissue growth

A schematic overview of the TOC device is presented in Figure 1A. The device design and microfabrication have been

**A**



**B**
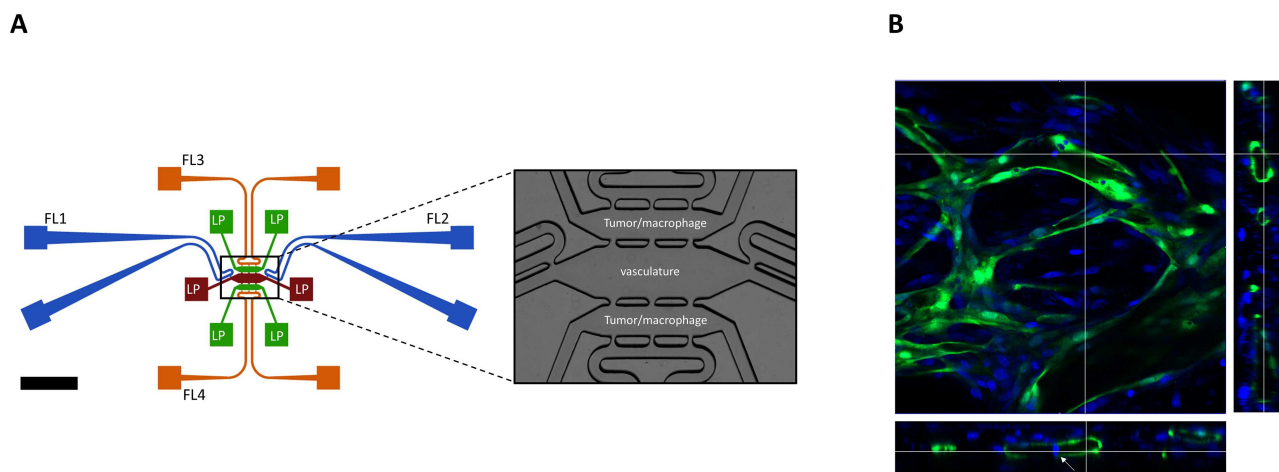


**Figure 1**. Schematic overview of the three chamber TOC device with tumor–vascular communication and 3D vasculature formed inside TOC device. (A) Endothelial cell precursors and fibroblasts are introduced into the central chamber (brown) through one of the connected loading ports (LP). Medium is added through fluidic lines (FL) on both ends of the central chamber (blue); the terminal ends of each FL are connected to a dedicated source and a sink (blue squares). Likewise, the upper and lower side chambers (green) each have LPs for introduction of tumor/other cells. The upper and lower chambers also have FLs (green) that can drain excess fluid. The central chamber is connected to the two parallel side chambers through pores that permit both cell and liquid transport (see enlarged image in the right panel). (B) Confocal images showed the 3D vasculature formed inside TOC device. Green: GFP-labeled endothelial cells. Blue: cell nucleus. White arrow: tumor cells inside the lumen of vasculature.

detailed previously [7]. The device pieces are bonded to a flat sheet of PDMS to seal the chambers and lines. The microvasculature in the central chamber was created by mixing ECFC-ECs and NHLFs at a 1:2 ratio in fibrin gel (bovine fibrinogen at a final concentration of 10 mg/ml and bovine plasma thrombin at a final concentration of 2 U/ml). The cells were maintained for 7 days in EGM-2 medium to permit development of the microvasculature (Fig. 1B). Tumor cells were loaded into the side chambers at a concentration of 5 million/ml suspended in 2.5 mg/ml growth factor reduced Matrigel™ (Corning) diluted with EGM-2 media. When introduced together with immune cells, the tumor cells and immune cells were mixed at a 1:1 ratio with a final cell concentration of 10 million/ml. Devices were kept at 37°C in 5% $CO_2$ for another 6–9 days and microscope images were taken on Days 2, 5 and 9 after loading of the side chambers.

### *In vitro* activation and differentiation of monocytic THP-1 and U-937 cell lines into macrophages

THP-1 and U-937 cells were cultured at $5 \times 10^5$ cells per well in 6-well plates and activated with PMA at a final concentration of 100 ng/ml for 48 hours. The cells were then washed to remove PMA and any unattached cells. For M1 macrophage differentiation, activated THP-1 and U-937 cells were cultured in 10 pg/ml LPS and 20 ng/ml IFN-$\gamma$ containing medium for 24 hours. For M2 macrophage differentiation, activated THP-1 or U-937 cells were kept in 20 ng/ml IL-4 and 20 ng/ml IL-13 for 72 hours (Supplementary Fig. S2, [16, 17]). Since M1 and M2 macrophage differentiation required different timeframes, monocytes were activated at different time points to synchronize the harvest of macrophages. Prior to introduction of macrophages into devices, aliquots of cells were stained with antibodies specific for cell markers of M1 and M2 macrophages and analyzed by flow cytometry. The remaining cells were counted and labeled with Violet CellTrace (Thermo Fisher Scientific, Waltham, MA) following the recommended protocol. Subsequently, macrophages were mixed with tumor cells and loaded into devices.

### Flow cytometry analysis

*In vitro* differentiated THP-1 or U-937 cells were harvested and then stained with antibodies specific for macrophage markers. Allophycocyanin (APC) anti-human CD68, APC/Cy7 anti-human tumor necrosis factor alpha (TNF-$\alpha$), Phycoerythrin (PE) anti-human CXCL10, Alexa Fluor 488 anti-human CD206 and PE/Cy7 anti-human interleukin-10 (IL-10) were used for analysis (all from BioLegend, San Diego, CA). The samples were run on an LSR Fortessa cell analyzer from BD (Becton Dickinson, Franklin Lakes, NJ). For analysis, initial gating was performed on expression of CD68 and positive cells were further analyzed for expression levels of individual markers. Unactivated THP-1 or U-937 cells were used as negative controls.

### Immunofluorescence, imaging and analysis

To perform immunofluorescence (IF) analysis on cells in devices, cells were fixed in 10% formalin for 48 hours. After washing with phosphate-buffered saline (PBS), cells were permeabilized with 0.2% Triton X-100 in PBS for another 48 hours. Then, primary antibodies or isotype control antibodies diluted in 1% bovine serum albumin (BSA)/PBS were added to devices and devices were kept at 4°C for 24 hours. Anti-von Willebrand factor (vWF, at 1:500 dilution), anti-ANGPT2 (at 1:500 dilution) and anti-tissue inhibitor matrix metalloproteinase 1 (TIMP1, at 1:1000 dilution) antibodies were all from Abcam (Branford, CT). After incubation with primary antibodies, devices were washed for 48 hours with PBS. Secondary antibody, goat anti-rabbit conjugated with Alexa Fluor 594 (Thermo Fisher Scientific, Waltham, MA) at 1:500 dilution was added to the devices. After 24 hours at 4°C, devices were washed again for 48 hours, and images were subsequently taken using an EVOS cell imaging system (Thermo Fisher Scientific, Waltham, MA). The vasculature and tumor areas were identified from their respective fluorescent areas in an image using ImageJ 1.52p. Tumor angiogenesis was assessed by measuring the microvessel area (GFP signals) in both side chambers or if no significant blood vessels grown into the side chambers, the ratio of blood
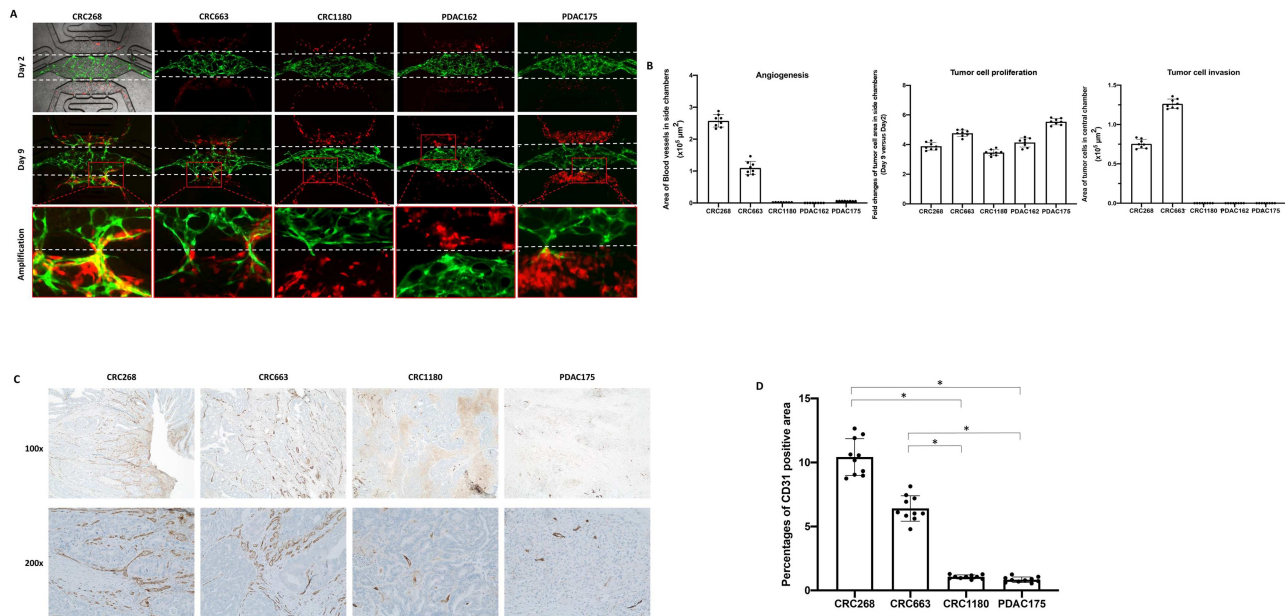
**Figure 2.** Vascularized TOC devices permit robust growth of colorectal and pancreatic cancer cells. Three CRC (CRC268, CRC663 and CRC1180) and two PDAC cell lines (PDAC162 and PDAC175) were introduced into the side chambers with preformed vasculature in the central chamber. (A) Representative IF images taken at Days 2 and 9 after tumor cells were introduced. Green: GFP-labeled endothelial cells formed vasculature. Red: RFP-labeled tumor cells. The white dotted lines indicate the top and bottom boundaries of the central chamber. (B) Quantification of angiogenesis, tumor cell proliferation and migration/invasion on Day 9. Eight devices per tumor cell line were used for quantification. (C) IHC images on parental CRC and PDAC tumor sections stained with anti-CD31. Representative images are shown at ×100 and ×200 magnifications. (D) Quantification of CD31-positive areas in parental tumors using IHC images. *$P < 0.05$.
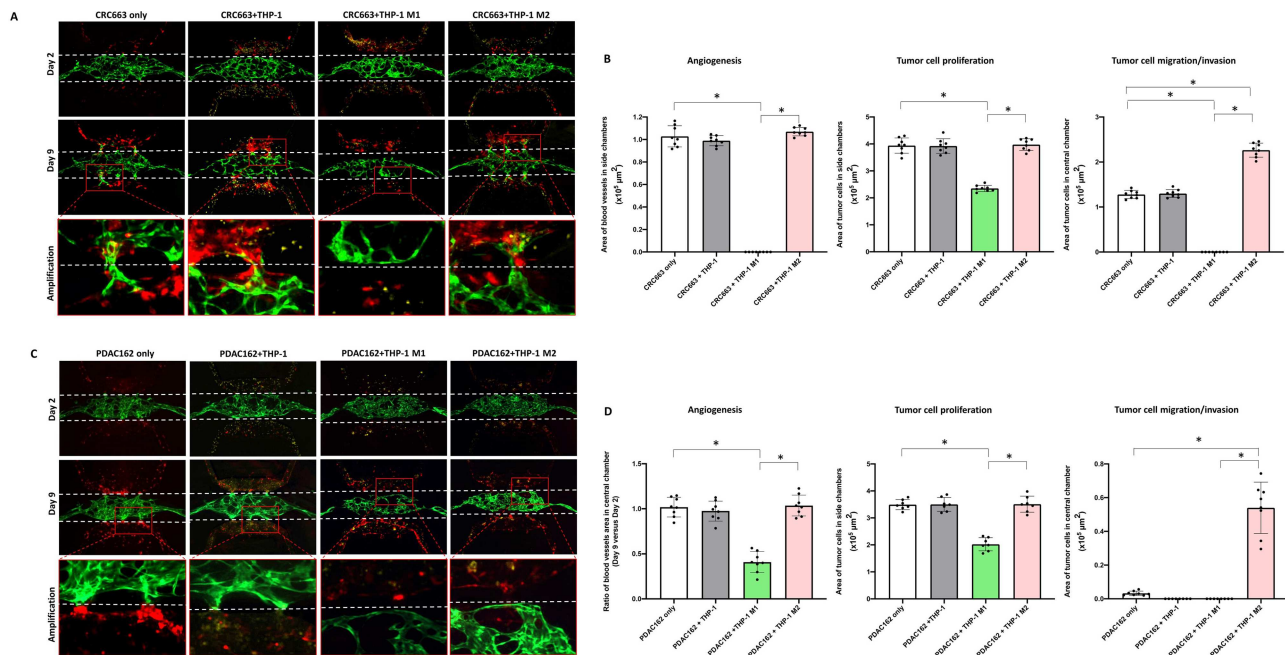


**Figure 3.** Reconstitution of M1- or M2-differentiated macrophages in TOC devices triggers antitumor and protumor phenotypes, respectively. (A, C) Representative IF images from Days 2 and 9 after CRC663 (A) or PDAC162 (C) cells with or without THP-1-derived macrophages were loaded into the side chambers. Green: GFP-labeled endothelial cells in preformed vasculature. Red: RFP-labeled tumor cells. Yellow dots: unactivated THP-1 cells or THP-1-derived M1 or M2 macrophages. White dotted line: the top and bottom boundaries of central chamber. Bottom panels represent amplified areas indicated by the red boxes in the middle panels. (B, D) Quantification of angiogenesis, tumor cell proliferation and tumor invasion in four types of TOC devices per tumor line. Eight devices per group were used for quantification. *$P < 0.05$.

vessel areas on Day 9 versus Day 2 in the central chamber was used as an alternative to show the vasculature density changes. Tumor cell proliferation was assessed by measuring the tumor cells area (RFP signals) in both side chambers and tumor invasion was assessed by measuring the tumor area (RFP signals) in the central chamber at the end of experiments.

## Immunohistochemistry

To perform immunohistochemistry (IHC) on formalin-fixed, paraffin-embedded human tissues, paraffin blocks of the samples were sectioned at 5 µm thickness and sections were mounted onto glass slides. After deparaffinization and rehydration, endogenous peroxidase was blocked with 0.3% $H_2O_2$ in methanol and then antigen retrieval was performed with a heated citrate buffer solution. Anti-CD31 (#JC70A, Agilent, Santa Clara, CA) was used to stain tissue sections. Horseradish Peroxidase (HRP) conjugated goat anti rabbit antibody (Abcam, Branford, CT) was then added and finally, DAB-substrate (Vector Laboratories, Burlingame, CA) was added for color development for 2 minutes at room temperature. Counter stain was performed with Mayer's hematoxylin (Thermo Fisher Scientific, Waltham, MA) and cover slips were mounted with Cytoseal XYL (Thermo Fisher Scientific, Waltham, MA).

## Protein analysis and antibody-mediated neutralization

Around 25–40 µl of flow through media was harvested per TOC device containing vasculature + CRC663 + THP-1 M1 or M2 macrophages. Three individual devices were used per condition, and media were pooled. All samples, as well medium controls, were subjected to analysis for soluble proteins using the immune–oncology test platform from Olink Proteomics (Uppsala, Sweden). Quality control and Normalized Protein Expression (NPX) values were generated by the company following their standard protocol. For neutralization of specific soluble factors, devices containing vasculature + CRC663 + THP-1 M1 or M2 macrophages were prepared as described above. Antibodies were added to the devices through the feeding medium. Specifically, antibodies to CXCL9 (clone 49106 at 0.5 µg/ml), CXCL10 (clone 33036 at 0.5 µg/ml) and CXCL11 (clone 87328 at 0.1 µg/ml) were added to devices with THP-1 M1 macrophages, whereas MMP7 (clone 111433 at 1 µg/ml) and ANGPT2 (clone 85816 at 1 µg/ml) (all from R&D systems, Minneapolis, MN) neutralizing antibodies were added to devices with THP-1 M2 macrophages. Medium and antibodies were changed every 48 hours.

## Cell harvest and scRNA-seq

Devices were washed with Dulbecco's phosphate-buffered saline (D-PBS) for three times and 20 U/ml nattokinase (Japan Bio Science Laboratory Company, JBSL-USA, Walnut Creek, CA) in D-PBS was added to the devices. After 20 minutes incubation at 37°C, cells were harvested from the devices with a pipette and transferred into a 1.5 ml Eppendorf tube. Cells were spun down and resuspended in 500 µl of 0.05% trypsin–ethylenediaminetetraacetic acid, followed by incubation at 37°C for 5 minutes. The cells were washed twice with D-PBS and resuspended in 0.04% BSA/PBS. Around 30 000 cells with a viability >80% were analyzed by scRNA-seq at the McDonnell Genome Institute at Washington University in St. Louis.

## scRNA-seq data analysis

For scRNA-seq analysis, Cell Ranger (v3.0.2) from 10× Genomics was used for demultiplexing sequence data into FASTQ files, aligning reads to the human genome (GRCh38) and generating gene-by-cell UMI count matrices. The R package Seurat (v3.1.0) was used for all subsequent analysis [18]. First, a series of quality filters were applied to the data to remove empty droplets/debris and dead cells. To do so, we set the minimum cut-off for number of features and UMI as 200 and 1000, respectively; we set the maximum cut-off for mitochondrial gene expression percentage as 10%. Next, the data were normalized and scaled. Highly variable genes are found for PCA-based feature selection. The cells were then clustered using graph-based clustering (default setting of Seurat). Cell types were assigned to each cluster by manually reviewing the expression of marker genes. The marker genes used were CD34, Platelet And Endothelial Cell Adhesion Molecule 1 (PECAM1), vWF (endothelial cells); GABA Type A Receptor-Associated Protein (GABARAP), prefoldin subunit 5 (PFDN5), Vascular Endothelial Growth Factor A (VEGFA), (tumor cells); Adrenomedullin (ADM), connective tissue growth factor (CTGF), Actin Alpha 2, Smooth Muscle (ACTA2) (stroma cells); CD68, colony stimulating factor 1 receptor (CSF1R), Membrane Spanning 4-Domains A7 (MS4A7) (macrophages). Integration was performed with the protocol from the Seurat package. To find differentially expressed genes between clusters of interest, the function FindMarkers was used with all parameters as default. All the genes returned from the FindMarkers function were treated as differentially expressed genes. For pathway analysis within endothelial cell clusters, cells from each cluster were pulled together for comparison regardless of devices of origin. Genes with absolute log-transformed fold change >0.6 were fed into the Reactome database to perform pathway enrichment analysis. Top enriched pathways are shown.

## Statistics

Statistical analysis was performed using one-way analysis of variance tests for multiple comparisons or Student's *t*-tests. All data were presented as the mean ± standard deviation. Results were considered statistically significant for $P < 0.05$.

## RESULTS

### Tumor cell lines demonstrate growth and heterogeneous induction of angiogenesis

The tumor cells lines were loaded into the side chambers of the devices after the microvascular network was formed in the central chamber (Fig. 1). Tumor cells were cultured for 9 days and proliferation was assessed. After normalization to the tumor area on Day 2, all five early passage tumor lines tested showed a 3–5-folds increase in tumor area by Day 9, indicating significant tumor growth (Fig. 2A, B). The increased tumor cell densities were not due to increases in tumor cell size, based on comparison of red fluorescence (tumor cells) in Days 2 and 9 images. Similar results were seen with the commercial tumor lines (Supplementary Fig. S1). Interestingly, different cell lines displayed diverse invasion capacity over time in the device. CRC663, SW480, and CRC268 tumor lines clearly invaded the vasculature in the central chamber (Fig. 2 and Supplementary Fig. S1). These cell lines also induced tumor angiogenesis as new vessels can be observed sprouting from the central chamber into the side (tumor) chambers through the pores between the central and side chambers. Conversely, CRC1180 and the two PDAC lines showed much less invasion and angiogenesis. The level of angiogenesis of tumor lines in TOC devices appeared to correlate with the density of the vascular marker, CD31, in matching parental tumors (Fig. 2C, D).

### M1 macrophages inhibit tumor invasion, growth and angiogenesis

To investigate the potential role of macrophages in modulating tumor growth and angiogenesis, we next differentiated

monocytic THP-1 cells into M1 or M2 macrophages (Supplementary Fig. S2). Flow cytometry analysis showed that after activation of THP-1 cells with PMA, >80% of the cells expressed the common macrophage marker CD68 (data not shown). Differentiation into M1 showed ~90% of the cells positive for CXCL10 and among these, ~48% cells were also positive for TNF-$\alpha$ (Supplementary Fig. S3A upper panel). Conversely, M2-differentiated macrophages expressed CD206 and IL-10 (Supplementary Fig. S3A, lower panel). Similar differentiation into M1/M2 macrophages was observed using the monocytic cell line, U937 (Supplementary Fig. S3B).

M1 macrophages derived from THP-1 were introduced together with CRC663 or PDAC162 two representative tumor cell lines into the side chambers of vascularized devices. CRC663 represented more aggressive and more angiogenetic tumors, whereas PDAC162 represented relative non-aggressive and non-angiogenetic tumors as shown in Figure 2. Over the course of 9 days, CRC663 showed induction of both angiogenesis and tumor invasion by itself (Fig. 3A, first column, B). In the presence of unactivated THP-1, there were no detectable differences compared with CRC663 tumor only (Fig. 3A, second column). However, in the presence of THP-1 M1, angiogenesis was completely blocked and the microvascular network in the central chamber started to recede by Day 9 (Fig. 3A, third column, B). At the same time, no tumor cells were detected in the central chamber at the end of the experiment (Day 9), indicating tumor migration/invasion was also inhibited. Additionally, tumor growth in the side chambers was significantly reduced compared with tumor-only devices (Fig. 3B). In summary, introduction of M1 macrophages triggered strong antitumor effects (inhibition of growth, migration and angiogenesis) in the devices. Similar phenotypic changes were observed when using PDAC162 tumor cells and THP-1 or THP-1 M1 (Fig. 3C, first three columns, D). U-937 M1 macrophages induced a very similar inhibitory antitumor phenotype when cocultured with CRC663 (Supplementary Fig. S4A, first two columns, B) or PDAC162 (Supplementary Fig. S4C, first two columns, D).

## M2 macrophages promote tumor cell migration

When M2 macrophages were introduced into devices, alongside tumor cells, tumor growth and angiogenesis were not impacted and were very similar to that observed in devices with tumors only or tumor plus unactivated macrophages (Fig. 3A, fourth column, B). However, tumor migration into the central chamber was significantly increased. More specifically, the number of CRC663 tumor cells in the central chamber at the end of the experiment (Day 9) was two times higher (Fig. 3A fourth column, B). The proinvasion effect of M2 macrophages on PDAC162 cells was particularly striking. The PDAC162 cells poorly migrated into the central chamber with or without unactivated macrophages, but in the presence of M2 macrophages the number of tumor cells in the central chamber increased by >10-fold (Fig. 3C fourth column, D). An increase in tumor migration into the central chamber was also observed when M2 macrophages were derived from the monocytic U937 cell line (Supplementary Fig. S4). Overall, a strong protumor effect of M2 macrophages was observed on both CRC and PDAC tumor cells.

## M1/M2 macrophage-derived soluble factors mediate anti/protumor effects.

To explore the mechanism for the observed anti/protumor effects of M1 and M2 macrophages, respectively, we collected the flow through medium from triplicate devices and subjected the medium to proteomics analysis. A total of 92 soluble factors, including biomarkers related to tumor immunity and tumor development, were included in a predesigned immune–oncology panel (Olink Proteomics). Out of the 92 biomarkers, 50 were detectable in at least one of the samples (Supplementary Table S1). Using the regular EGM-2 medium as a negative control, relative quantitation was performed between CRC663 + THP-1 M1 versus CRC663 + THP-1 M2 macrophage samples. CXCL9 (~50×), CXCL10 (~70×) and CXCL11 (~3×) were dramatically increased in TOC devices containing THP-1 M1 macrophages (Fig. 4A). In contrast, in TOC devices containing THP-1 M2 macrophages, MMP7, ANGPT2, CC chemokine ligand (CCL) 3 and colony stimulating factor (CSF)-1 were significantly increased with MMP7 increased >7 times and ANGPT2 increased 20 times compared with the samples from THP-1 M1-TOC devices (Fig. 4A).

To test whether the differentially expressed soluble factors were directly responsible for the observed anti/protumor effects, we used neutralization antibodies. Mixed neutralization antibodies to CXCL9, CXCL10 and CXCL11 eliminated the antitumor phenotype observed in the presence of M1 macrophages (Fig. 4B). For example, the microvascular network area in the central chamber of THP-1 M1 TOC devices was decreased by <10% on Day 9 compared with Day 2 in the presence of the antibodies, whereas in the untreated devices, the area of microvascular network on Day 9 decreased >50% compared with Day 2. Additionally, tumor cell proliferation was restored with nearly twice as many tumor cells in the presence of antibodies (Fig. 4B).

A similar reversal of phenotype was observed when neutralizing antibodies to MMP7 and ANGPT2 were added to TOC devices with THP-1 M2 macrophages (Fig. 4C). Although there was no detectable change in the level of angiogenesis, the number of tumor cells that invaded the central chamber was reduced by one-third in the presence of anti-MMP7 and anti-ANGPT2 antibodies (Fig. 4C). Together, these data demonstrate that soluble mediators induced by the addition of macrophages to TOC devices including CXCL9, CXCL10, CXCL11, MMP7 and ANGPT2 contribute to the observed anti/protumor effects of M1 and M2 macrophages, respectively.

## scRNA-seq identifies gene expression profiles in endothelial cells driven by tumor cells and M2 macrophages

To more deeply understand the TOC devices with higher cellular resolution, cells were harvested from devices, processed into single-cell suspensions and subjected to scRNA-seq. We focused on devices with vasculature only, vasculature + tumor and vasculature + tumor + M2 macrophages. TOC devices with THP-1 M1 macrophages were omitted due to the substantial anti-angiogenic effect (Fig. 3) that would negatively impact the cell yield. As depicted in Figure 5A, all the cell types introduced in devices were recovered in the scRNA-seq data, which indicate that all cell types were viable in the TOC. Within individual cell types, it appeared there were multiple clusters per cell type. When Uniform Manifold Approximation and Projection (UMAP) data plots of the three different types of devices were merged, the pattern of the cell clusters detected was generally similar, but did not entirely overlap, suggesting that the gene expression profiles of cells recovered from different device compositions were not the same. Introduction of tumor cells into a vascularized device triggered both upregulation and downregulation of many genes in both endothelial cells and fibroblasts
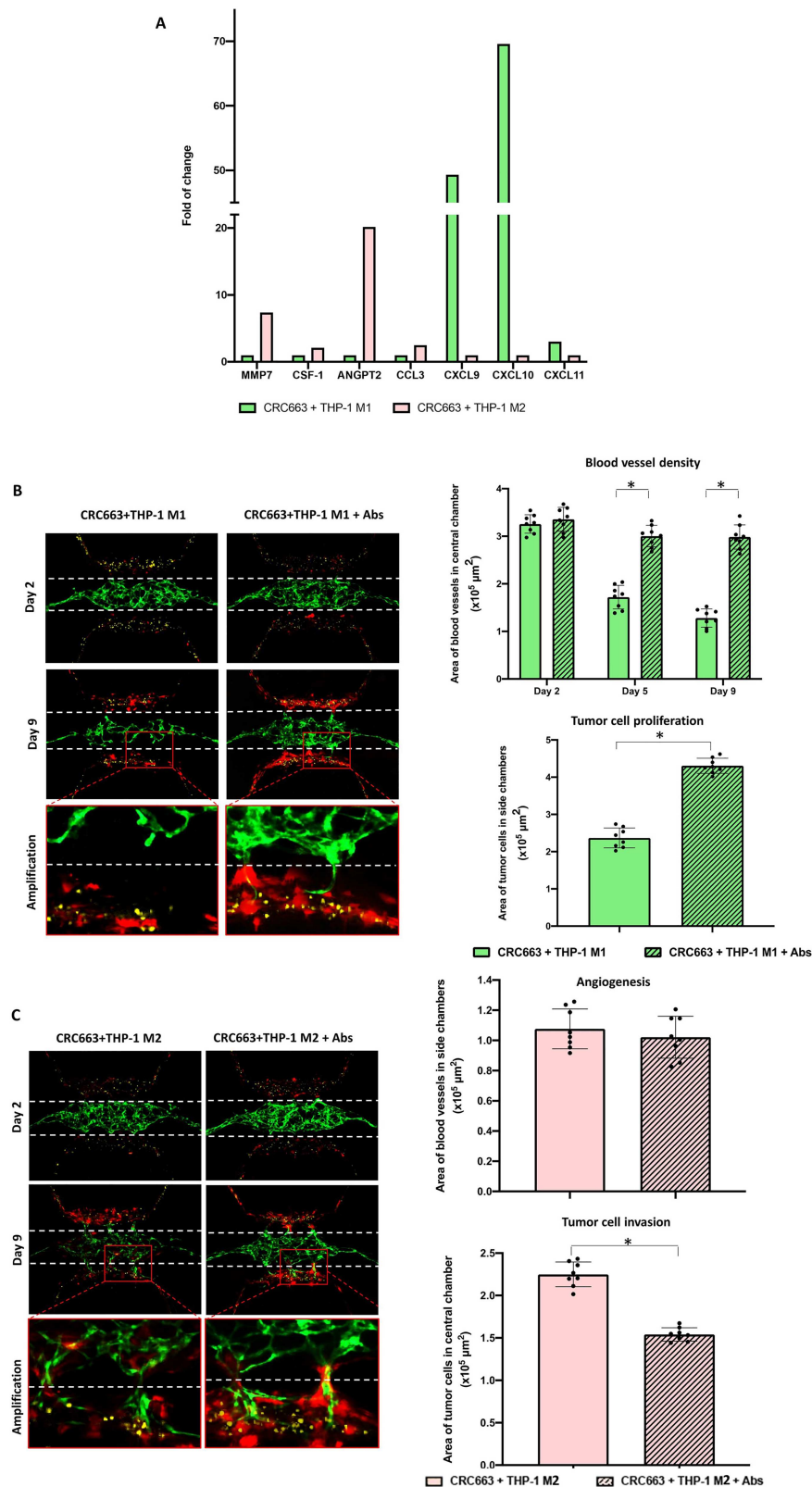
**Figure 4.** Analysis of soluble factors in M1 versus M2 macrophage-containing TOC devices shows macrophage-mediated antitumor and protumor effects, respectively. (A) The proteomic analysis of soluble factors recovered from TOC devices was performed. (B) Antibody-mediated neutralization of chemokines in M1 TOC devices. Left panel: representative images from Days 2 and 9 of CRC663 + M1 macrophage TOC devices with or without anti-CXCL9, anti-CXCL10 and CXCL-11 neutralizing antibodies. Green: GFP-labeled endothelial cells. Red: RFP-labeled CRC663 tumor cells. Blue: THP-1 derived M1 macrophages. White dotted line: the top and bottom boundaries of the central chamber. Right panels: quantification of blood vessel density in the central chamber on Days 2, 5 and 9 (top panel) and tumor cell proliferation in CRC663 TOC devices with M1 macrophages on Day 9 (bottom panel). (C) Antibody-mediated neutralization of chemokines in M2 TOC devices. Left panel: representative images from Days 2 and 9 of CRC663 + M2 macrophage TOC devices with or without anti-MMP7 and anti-ANGPT2 neutralizing antibodies. Green: GFP-labeled endothelial cells. Red: RFP-labeled CRC663 tumor cells. Yellow: THP-1 derived M2 macrophages. White dotted line: the top and bottom boundaries of the central chamber. Right panels: quantification of blood vessel density in side chambers on Day 9 (top panel) and tumor cell invasion in CRC663 TOC devices with M2 macrophages on Day 9 (bottom panel). Eight devices per group were used for quantification. *$P < 0.05$.
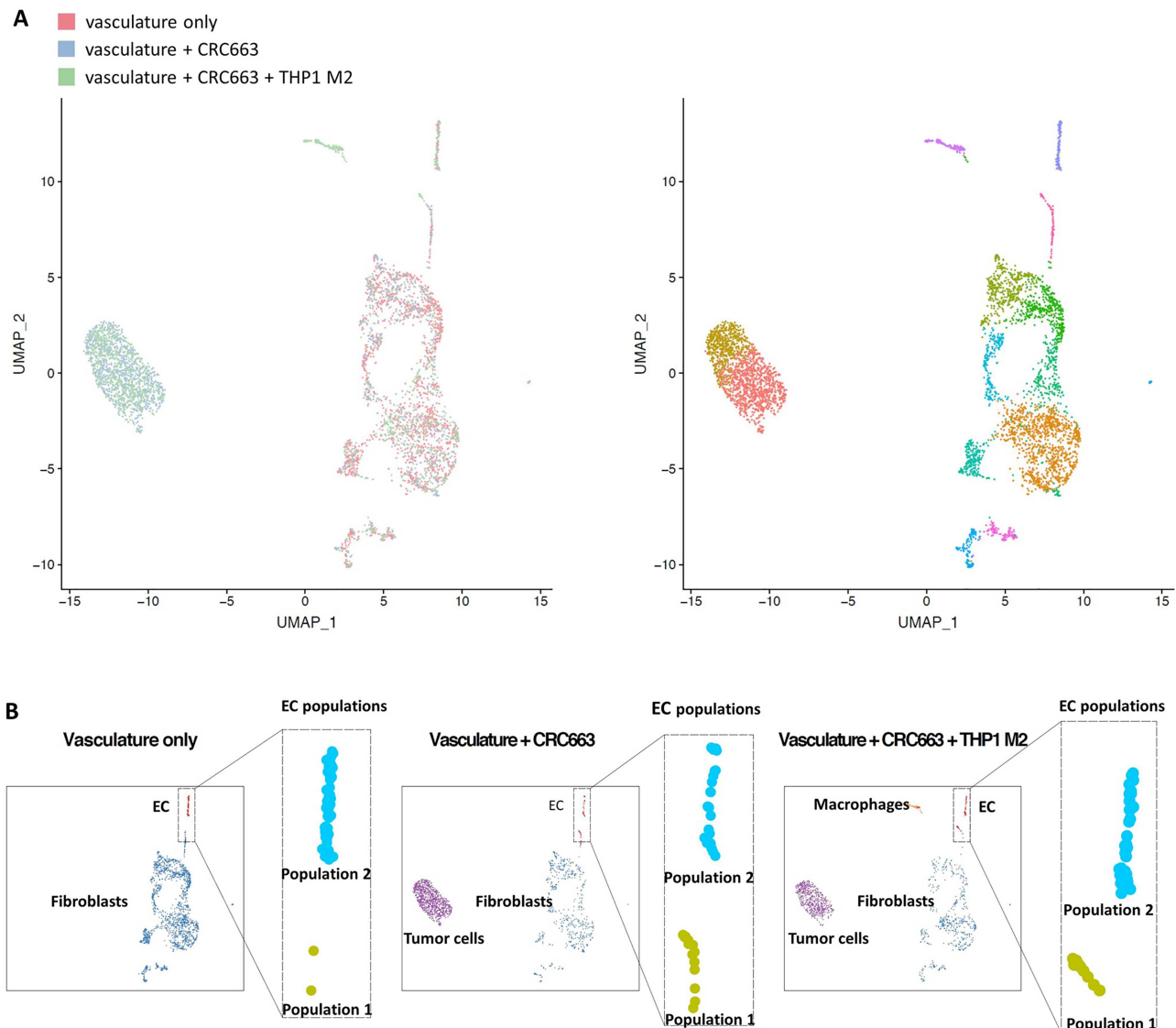
**Figure 5.** scRNA-seq analysis of TOC devices. (A) Left panel: integrated images of scRNA-seq data of all cells recovered from three groups of TOC devices: vasculature only, vasculature + CRC663 and vasculature + CRC663 + THP-1 M2 macrophages. Right panel: integrated images of subclusters of cells based on the similarities of their gene expression profiles. (B) Normalized individual images of cells recovered from each TOC, focused on endothelial cell clusters.

(Supplementary Fig. S5). The addition of THP-1 M2 macrophages dramatically impacted gene expression in both endothelial cells and fibroblasts. The gene expression changes were most pronounced in the endothelial cells. For example, the presence of THP-1 M2 created a heterogeneous endothelial cell phenotype when tumor cells were also present (Fig. 5B). One of the endothelial cell clusters, P2, appeared similar in all three types of devices; a second cluster (P1) was clearly distinct from the first cluster and larger in the presence of THP-1 M2 macrophages and tumor. These data suggest that the differences between the two endothelial cell clusters were induced by tumor cells and further enhanced in the presence of protumor THP-1 M2 macrophages.
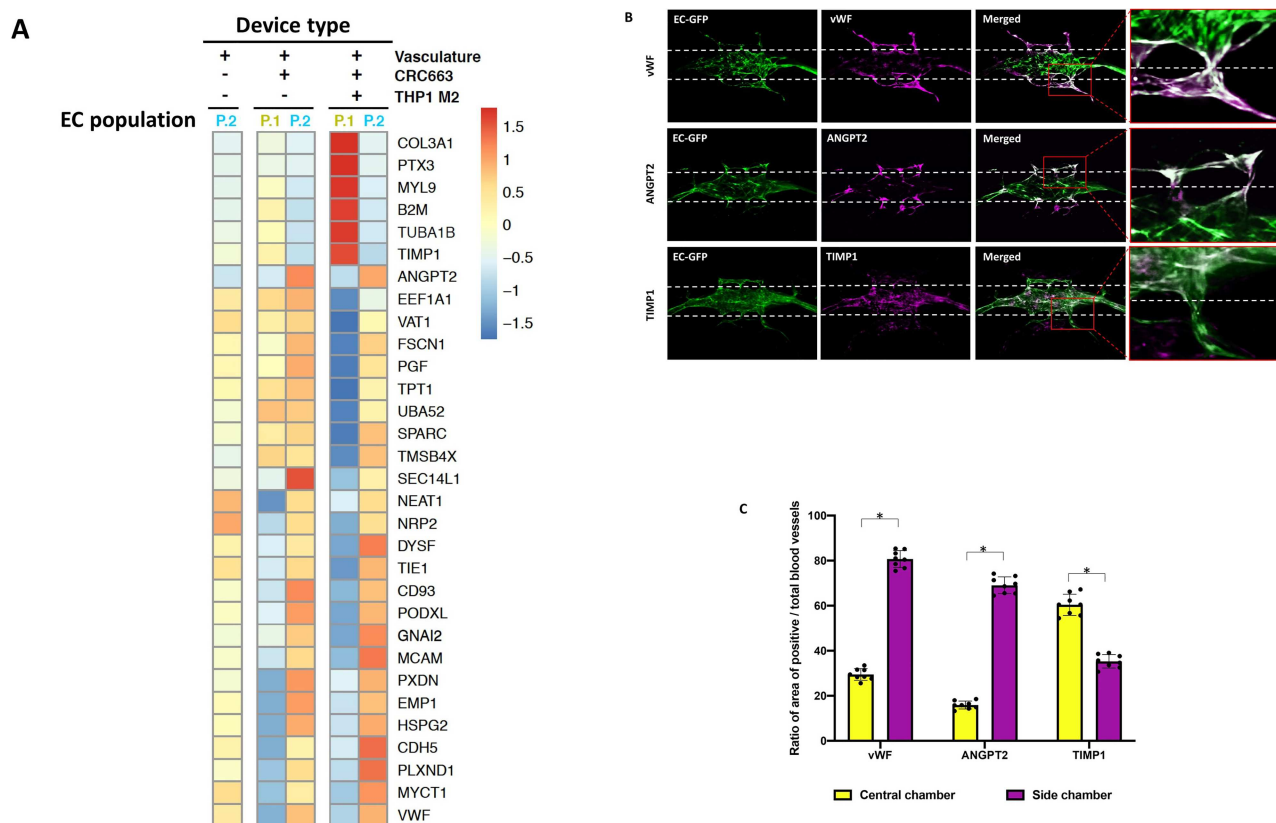
## Distinct gene expression profiles in endothelial cells reflect different levels of angiogenic activity

To assess in more detail what changes tumor cells and M2 macrophages induce in endothelial cells, we compiled an abbreviated list of genes that were most differentially expressed in the two endothelial cell clusters across three different devices. A heat map was compiled of 31 genes that were most significantly changed out of >1000 differentially expressed genes comparing the three different device conditions: vasculature only, vasculature with tumor and vasculature with tumor and THP-1 M2 macrophages (Fig. 6A). Differentially expressed genes between the P1 and P2 endothelial clusters are evident when THP-1 M2 macrophages were present (Fig. 6A). Pathway analysis revealed that the genes highly expressed in endothelial cluster P1 were related to cell cycle and immune pathways, whereas the genes highly expressed in endothelial cluster P2 were related to tumor development and tumor invasion pathways (Supplementary Fig. S6).

We next investigated whether the endothelial cells in P1 and P2 clusters had a distinct spatial distribution within the device. We chose to analyze two genes (*vWF* and *ANGPT2*) that were highly expressed in cluster P2 and one gene (*TIMP1*) that

Figure 6. Distinct gene expression profiles in endothelial cells reflect different levels of angiogenic activity. (A) Heat map of the most significantly differentially expressed genes in P1 and P2 endothelial cell clusters across all three groups. (B) vWF, ANGPT2 and TIMP1 IF images of vasculature + CRC663 + THP-1 M2 devices taken on Day 9. Green: GFP-labeled endothelial cells. Red: RFP-labeled CRC663 tumor cells. Magenta: vWF/ANGPT2/TIMP1 signal. Merged: image overlap of all three channels. (C) Quantification of the ratio of the vWF/ANGPT2/TIMP1-positive vasculature area (the overlapping area of magenta and green signals) versus total vasculature area (total green signals) in the central chamber and both side chambers. Eight devices were used for quantification. *P < 0.05.

was highly expressed in P1. IF analysis of vWF and ANGPT2 in TOC devices seeded with M2 macrophages showed that the expression of these proteins was enhanced in the microvessels present in the tumor chamber and in some areas in the central chamber where blood vessels had sprouted (Fig. 6B, C). In contrast, endothelial cells with enhanced expression of TIMP1 were mainly located in the central chamber. These data suggest that the P1 and P2 endothelial clusters correspond to stable blood vessels and those engaged in active angiogenesis, respectively.

## DISCUSSION

We recently reported on the design and initial validation of a novel microfluidic TOC model in which tumor cells can survive and grow in a vascularized environment [7]. Herein, we extend this model in the current report by utilizing our TOC device to investigate the role of macrophages on tumor progression. Using patient-derived tumor cell lines from PDAC and CRC, we discovered that macrophages with a predominant M1 phenotype create an antitumor microenvironment that inhibits tumor growth, migration and angiogenesis, whereas a predominant M2 phenotype creates a protumor microenvironment that stimulates tumor growth, migration and angiogenesis. The antitumor behavior is mediated in part by chemokines CXCL9, CXCL10, CXCL11, whereas the protumor behavior is mediated in part by MMP7 and ANGPT2. Using scRNA-seq, we were able to identify two distinct endothelial cell phenotypes created by the presence

of the M1 and M2 macrophages in the presence of tumor cells and map these phenotypes to regions of the tumor microenvironment that reflect stable vessels and active angiogenesis, respectively. We conclude that our TOC model is able to recapitulate important features of the tumor immune and vascular microenvironments and can be used to understand the mechanisms by which the immune response can inhibit or stimulate tumor progression.

Tumors are complex mixtures of primarily tumor cells, leukocytes, stromal cells (e.g. cancer-associated fibroblasts) and blood vessels. There is ample evidence that each of these major cell types impacts tumor progression. In addition, the spatial and temporal relationships between these cells impact their function and further increase the complexity of the tumor microenvironment. It is difficult to tease apart these mechanistic relationships in small animal models, and traditionally, in vitro cancer modeling has relied on analysis of tumor cells grown in 2D cell culture. By their 2D and static design, these systems do not reconstitute the in vivo cellular microenvironment and mechanical properties found in vivo. The recent introduction of tumor organoid/spheroid models, including heterotypic models containing multiple types of cells, has dramatically improved our ability of to grow tumors under more natural conditions [19–21]. However, for questions related to dynamic tumor processes, such as angiogenesis, models that contain a dynamic, vascularized tumor microenvironment are required. While some groups have performed cocultures of endothelial cells and tumor cells or tumor spheres in microfluidic devices, these models do

not fully recapitulate the tumor vascular network [22–26]. Our group has developed various iterations of 3D perfused vascular networks [27–29], including the current device that includes the ability to introduce and combine different cell types within the tumor microenvironment with spatial and temporal control [7]. Tumor cells and other types of cells can be introduced in two chambers that are connected to a central chamber containing an intact, preformed and perfused living vascular network. Cells are resuspended in Matrigel to provide a 3D matrix. While most tumors readily grow inside TOC devices, our current studies also show that tumor behavior in TOC devices recapitulates important features of the parental tumors. Some tumors (CRC268, CRC663) showed enhanced angiogenesis as well as high levels of tumor migration/invasion, whereas others showed lower levels of angiogenesis and migration. These phenotypes resembled the corresponding *in vivo* pathological features observed in the corresponding parental tumors. Additionally, control devices with normal cells or Matrigel only added to the side chamber did not show angiogenesis, adding to the biological relevance of the observations.

Other research groups have presented similar microfluidic TOC models containing perfused vasculature to study tumor-induced angiogenesis and drug delivery [30–35]. Most models use endothelial cells or precursors in a matrix consisting of collagen or fibrin; tumor cell lines or tumor spheroids in an adjacent compartment separated from the endothelial cells through a porous membrane and microfluidic lines. Considerations for the basic design include the need for a self-organizing, perfusable vascular network, a hydrogel matrix and microfluidic lines to establish gradients of soluble factors. Another consideration is the cell density in TOC devices that should resemble the high cell density in *in vivo* tissues. The development of microfluidic-based 3D cell culture models to study tumor biology has gained a lot of attention in the last several years, in particular through the parallel improvements in establishing tumor organoids that can be introduced into TOC devices. Many papers, including several excellent reviews [33, 35], have been published on both important developments in microfluidic 3D cultures, as well as comparisons of microfluidic models [35, 36]. Together, these studies have demonstrated the importance of vascular network flow in evaluating tumor progression, and suggest that vascularized TOC models could be ideal *in vitro* models for personalized cancer research while complementing other *in vitro* or *in vivo* models.

We used our vascularized TOC to investigate mechanisms by which macrophages impact tumor progression. Of all immune cell subsets, macrophages, in particular the M2 phenotype, have been proven to be crucial drivers of chronic cancer-associated inflammation and are involved in almost every step of cancer progression [37, 38] and have been implicated in driving resistance to therapy [39, 40]. Tumor-associated macrophages are associated with the M2 phenotype and are generally recognized as potential biomarkers for diagnosis and prognosis of cancer, as well as potential therapeutic targets for cancer [41–44]. M1 macrophages, on the other hand, have antitumor properties. Pre-polarized M1 or M2 macrophages from two different monocyte cell lines (THP-1 and U-937) remained viable in our TOC devices throughout the experiments and triggered cellular behavior in the tumor microenvironment through soluble factors consistent with previous reports [45, 46]. While our experimental design does not allow to conclude that macrophages produced the soluble factors, our data clearly suggest they triggered the biological changes. Specifically, devices with M1 macrophages showed

strong antitumor effects such as the degradation of vasculature and reduced tumor cell proliferation and migration. These observations were due, in part, to the production of CXCL9, CXCL10 and CXCL11 that can inhibit angiogenesis induced by VEGF and basic fibroblast growth factor (bFGF) by interacting with a common receptor, CXCR3, on endothelial cells [47–49]. Macrophage-derived CXCL9 and CXCL10 have also been shown to be critically important for antitumor immune responses [9]. In contrast, devices loaded with M2 macrophages showed significant protumor effects including an increase in angiogenesis and tumor migration/invasion that was associated with increased production of MMP7 and ANGPT2. MMP7 expression in CRCs is increased and has been shown to promote metastasis through degradation of the extracellular matrix and E-cadherin [14, 50, 51]. Similarly, ANGPT2 is well known to have proangiogenic and protumor activity, as well as to function in resistance to anti-VEGF therapy [52–54]. Although the neutralization of these two soluble factors showed no significant difference in angiogenesis, tumor invasion was dramatically decreased in the presence of the neutralization antibodies. Of note, while control antibodies were not tested in this experimental set-up, isotype-matched control antibodies used for fluorescent imaging of cells/markers in TOC devices (Fig 6B) did not bind non-specifically. We did not assess macrophage migration, but Lee *et al.* [55], using a dual-compartment, non-vascularized microfluidic coculture device, recently demonstrated that macrophage migration is induced by interstitial flow or through IL8 and CCL2 in the presence of pancreas tumor cells.

Insight into the molecular mechanisms of the observed tumor phenotypes in our TOC was performed through scRNA-seq. All cell types were successfully recovered from the TOC and identified by scRNA-seq. We were able to demonstrate that introduction of tumor cells and M2 macrophages created two endothelial cell clusters with >1000 differentially expressed genes. The differences in enriched pathway of the differentially expressed genes between the two endothelial populations (Supplementary Fig. S5) suggest further functional or biological relevance of these two populations. One endothelial cell population expressed high proangiogenic markers, whereas the other expressed more antiangiogenic markers. In particular, vWF and ANGPT2, two well-known factors involved in endothelial cell activation and tumor angiogenesis [56–60], were highly expressed in the endothelial cell population located spatially in the tumor compartment, whereas TIMP1, a known antiangiogenic marker [61, 62], was expressed in the endothelial cells present mostly in the vascular chamber. The gene expression profiles and functional status of these two endothelial cell populations may allow us to better understand the relationship between inflammation and endothelial cells during tumor progression and provide potential therapeutic targets for tumor treatments.

In conclusion, our data strongly suggest that our vascularized TOC creates a tumor microenvironment that is biologically relevant and recapitulates key features of parental tumors. The TOC can be used to probe mechanisms by which the immune system impacts tumor growth. Our results show that M1 and M2 macrophages secrete distinct profiles of soluble factors that include CXCL9, CXCL10, CXCL11, MMP7 and ANGPT2 that can dramatically alter tumor cell proliferation and migration, as well as endothelial cell phenotype. The TOC model is not limited to the use of tumor cell lines [7], but can also provide insight into personalized and precision cancer treatments, including cancer immunotherapy.

## SUPPLEMENTARY DATA

Supplementary data are available at *INTBIO* Journal online.

## CONFLICT OF INTEREST

S.C.G. has equity in Aracari Biosciences, a startup company whose core technology involves perfused human microvessels. There are no conflicts to declare for all other authors.

## REFERENCES

1. Ostuni R, Kratochvill F, Murray PJ *et al* Macrophages and cancer: from mechanisms to therapeutic implications. *Trends Immunol* 2015;**36**:229–39.
2. Yang M, McKay D, Pollard JW *et al* Diverse functions of macrophages in different tumor microenvironments. *Cancer Res* 2018;**78**:5492–503.
3. Cortese N, Soldani C, Franceschini B *et al* Macrophages in colorectal cancer liver metastases. *Cancers (Basel)* 2019;**11**:633.
4. Farajzadeh Valilou S, Keshavarz-Fathi M, Silvestris N *et al* The role of inflammatory cytokines and tumor associated macrophages (TAMs) in microenvironment of pancreatic cancer. *Cytokine Growth Factor Rev* 2018;**39**:46–61.
5. Italiani P, Boraschi D. From monocytes to M1/M2 macrophages: phenotypical vs. functional differentiation. *Front Immunol* 2014;**5**:514.
6. Shapouri-Moghaddam A, Mohammadian S, Vazini H *et al* Macrophage plasticity, polarization, and function in health and disease. *J Cell Physiol* 2018;**233**:6425–40.
7. Shirure VS, Bi Y, Curtis MB *et al* Tumor-on-a-chip platform to investigate progression and drug sensitivity in cell lines and patient-derived organoids. *Lab Chip* 2018;**18**:3687–702.
8. Hanahan D, Weinberg RA. Hallmarks of cancer: the next generation. *Cell* 2011;**144**:646–74.
9. Tokunaga R, Zhang W, Naseem M *et al* CXCL9, CXCL10, CXCL11/CXCR3 axis for immune activation - a target for novel cancer therapy. *Cancer Treat Rev* 2018;**63**:40–7.
10. Abron JD, Singh NP, Murphy AE *et al* Differential role of CXCR3 in inflammation and colorectal cancer. *Oncotarget* 2018;**9**:17928–36.
11. Huang H, Bhat A, Woodnutt G *et al* Targeting the ANGPT-TIE2 pathway in malignancy. *Nat Rev Cancer* 2010;**10**:575–85.
12. Jary M, Hasanova R, Vienot A *et al* Molecular description of ANGPT2 associated colorectal carcinoma. *Int J Cancer* 2020;**147**:2007–18.
13. Puchert M, Obst J, Koch C *et al* CXCL11 promotes tumor progression by the biased use of the chemokine receptors CXCR3 and CXCR7. *Cytokine* 2020;**125**:154809.
14. Basu S, Thorat R, Dalal SN. MMP7 is required to mediate cell invasion and tumor formation upon Plakophilin3 loss. *PLoS One* 2015;**10**:e0123979.
15. Shirure VS, Lezia A, Tao A *et al* Low levels of physiological interstitial flow eliminate morphogen gradients and guide angiogenesis. *Angiogenesis* 2017;**20**:493–504.
16. Smith MP, Young H, Hurlstone A *et al* Differentiation of THP1 cells into macrophages for transwell co-culture assay with melanoma cells. *Bio Protoc* 2015;**5**:e1638.
17. Baxter EW, Graham AE, Re NA *et al* Standardized protocols for differentiation of THP-1 cells to macrophages with distinct M(IFNgamma+LPS), M(IL-4) and M(IL-10) phenotypes. *J Immunol Methods* 2020;**478**:112721.
18. Butler A, Hoffman P, Smibert P *et al* Integrating single-cell transcriptomic data across different conditions, technologies, and species. *Nat Biotechnol* 2018;**36**:411–20.
19. Fan H, Demirci U, Chen P. Emerging organoid models: leaping forward in cancer research. *J Hematol Oncol* 2019;**12**:142.
20. Weiswald LB, Bellet D, Dangles-Marie V. Spherical cancer models in tumor biology. *Neoplasia* 2015;**17**:1–15.
21. Boj SF, Hwang CI, Baker LA *et al* Organoid models of human and mouse ductal pancreatic cancer. *Cell* 2015;**160**:324–38.
22. Lee JH, Kim SK, Khawar LA *et al* Microfluidic co-culture of pancreatic tumor spheroids with stellate cells as a novel 3D model for investigation of stroma-mediated cell motility and drug resistance. *J Exp Clin Cancer Res* 2018;**37**:1–12.
23. Han B, Qu CJ, Park K *et al* Recapitulation of complex transport and action of drugs at the tumor microenvironment using tumor-microenvironment-on-chip. *Cancer Lett* 2016;**380**:319–29.
24. Bhatia SN, Ingber DE. Microfluidic organs-on-chips. *Nat Biotechnol* 2014;**32**:760–72.
25. Nguyen DHT, Lee E, Alimperti S *et al* A biomimetic pancreatic cancer on-chip reveals endothelial ablation via ALK7 signaling. *Sci Adv* 2019;**5**:eaav6789.
26. Aref AR, Huang RYJ, Yu WM *et al* Screening therapeutic EMT blocking agents in a three-dimensional microenvironment. *Integr Biol-UK* 2013;**5**:381–9.
27. Alonzo LF, Moya ML, Shirure VS *et al* Microfluidic device to control interstitial flow-mediated homotypic and heterotypic cellular communication. *Lab Chip* 2015;**15**:3521–9.
28. Ehsan SM, Welch-Reardon KM, Waterman ML *et al* A three-dimensional in vitro model of tumor cell intravasation. *Integr Biol-UK* 2014;**6**:603–10.
29. Moya M, Tran D, George SC. An integrated in vitro model of perfused tumor and cardiac tissue. *Stem Cell Res Ther* 2013;**4**:1–6.
30. Chung M, Ahn J, Son K *et al* Biomimetic model of tumor microenvironment on microfluidic platform. *Adv Healthc Mater* 2017;**6**:1700196.
31. Nashimoto Y, Hayashi T, Kunita I *et al* Integrating perfusable vascular networks with a three-dimensional tissue in a microfluidic device. *Integr Biol-UK* 2017;**9**:506–18.

32. Nashimoto Y, Okada R, Hanada S *et al* Vascularized cancer on a chip: The effect of perfusion on growth and drug delivery of tumor spheroid. *Biomaterials* 2020;**229**:119547.

33. van Duinen V, Trietsch SJ, Joore J *et al* Microfluidic 3D cell culture: from tools to tissue models. *Curr Opin Biotechnol* 2015;**35**:118–26.

34. Zheng Y, Chen JM, Craven M *et al* In vitro microvessels for the study of angiogenesis and thrombosis. *P Natl Acad Sci USA* 2012;**109**:9342–7.

35. Osaki T, Sivathanu V, Kamm RD. Vascularized microfluidic organ-chips for drug screening, disease models and tissue engineering. *Curr Opin Biotechnol* 2018;**52**:116–23.

36. Coughlin MF, Kamm RD. The use of microfluidic platforms to probe the mechanism of cancer cell extravasation. *Adv Healthc Mater* 2020;**9**:e1901410.

37. Chen Y, Song Y, Du W *et al* Tumor-associated macrophages: an accomplice in solid tumor progression. *J Biomed Sci* 2019;**26**:78.

38. Chanmee T, Ontong P, Konno K *et al* Tumor-associated macrophages as major players in the tumor microenvironment. *Cancers (Basel)* 2014;**6**:1670–90.

39. Noy R, Pollard JW. Tumor-associated macrophages: from mechanisms to therapy. *Immunity* 2014;**41**:49–61.

40. Fu XT, Song K, Zhou J *et al* Tumor-associated macrophages modulate resistance to oxaliplatin via inducing autophagy in hepatocellular carcinoma. *Cancer Cell Int* 2019;**19**:71.

41. Cassetta L, Pollard JW. Targeting macrophages: therapeutic approaches in cancer. *Nat Rev Drug Discov* 2018;**17**:887–904.

42. Genard G, Lucas S, Michiels C. Reprogramming of tumor-associated macrophages with anticancer therapies: radiotherapy versus chemo- and immunotherapies. *Front Immunol* 2017;**8**:828.

43. Lin Y, Xu J, Lan H. Tumor-associated macrophages in tumor metastasis: biological roles and clinical therapeutic applications. *J Hematol Oncol* 2019;**12**:76.

44. Petty AJ, Yang Y. Tumor-associated macrophages: implications in cancer immunotherapy. *Immunotherapy* 2017;**9**:289–302.

45. Sawa-Wejksza K, Dudek A, Lemieszek M *et al* Colon cancer-derived conditioned medium induces differentiation of THP-1 monocytes into a mixed population of M1/M2 cells. *Tumour Biol* 2018;**40**:1010428318797880.

46. Genin M, Clement F, Fattaccioli A *et al* M1 and M2 macrophages derived from THP-1 cells differentially modulate the response of cancer cells to etoposide. *BMC Cancer* 2015;**15**:577.

47. Bodnar RJ, Yates CC, Rodgers ME *et al* IP-10 induces dissociation of newly formed blood vessels. *J Cell Sci* 2009;**122**:2064–77.

48. Bodnar RJ, Yates CC, Wells A. IP-10 blocks vascular endothelial growth factor-induced endothelial cell motility and tube formation via inhibition of calpain. *Circ Res* 2006;**98**:617–25.

49. Wilson NO, Solomon W, Anderson L *et al* Pharmacologic inhibition of CXCL10 in combination with anti-malarial therapy eliminates mortality associated with murine model of cerebral malaria. *Plos One* 2013;**8**:e60898.

50. Polistena A, Cucina A, Dinicola S *et al* MMP7 expression in colorectal tumours of different stages. *In Vivo* 2014;**28**:105–10.

51. Yu B, Liu X, Chang H. MicroRNA-143 inhibits colorectal cancer cell proliferation by targeting MMP7. *Minerva Med* 2017;**108**:13–9.

52. Wu X, Giobbie-Hurder A, Liao X *et al* Angiopoietin-2 as a biomarker and target for immune checkpoint therapy. *Cancer Immunol Res* 2017;**5**:17–28.

53. Scholz A, Plate KH, Reiss Y. Angiopoietin-2: a multifaceted cytokine that functions in both angiogenesis and inflammation. *Ann N Y Acad Sci* 2015;**1347**:45–51.

54. Schmittnaegel M, Rigamonti N, Kadioglu E *et al* Dual angiopoietin-2 and VEGFA inhibition elicits antitumor immunity that is enhanced by PD-1 checkpoint blockade. *Sci Transl Med* 2017;**9**:eaak9670.

55. Lee SWL, Seager RJ, Litvak F *et al* Integrated in silico and 3D in vitro model of macrophage migration in response to physical and chemical factors in the tumor microenvironment. *Integr Biol (Camb)* 2020;**12**:90–108.

56. Damin DC, Rosito MA, Gus P *et al* Von Willebrand factor in colorectal cancer. *Int J Colorectal Dis* 2002;**17**:42–5.

57. Zanetta L, Marcus SG, Vasile J *et al* Expression of Von Willebrand factor, an endothelial cell marker, is up-regulated by angiogenesis factors: a potential method for objective assessment of tumor angiogenesis. *Int J Cancer* 2000;**85**:281–8.

58. Lackner C, Jukic Z, Tsybrovskyy O *et al* Prognostic relevance of tumour-associated macrophages and von Willebrand factor-positive microvessels in colorectal cancer. *Virchows Arch* 2004;**445**:160–7.

59. Lewis CE, De Palma M, Naldini L. Tie2-expressing monocytes and tumor angiogenesis: Regulation by hypoxia and angiopoietin-2. *Cancer Res* 2007;**67**:8429–32.

60. Biel NM, Siemann DW. Targeting the Angiopoietin-2/Tie-2 axis in conjunction with VEGF signal interference. *Cancer Lett* 2016;**380**:525–33.

61. Hornebeck W, Lambert E, Petitfrere E *et al* Beneficial and detrimental influences of tissue inhibitor of metalloproteinase-1 (TIMP-1) in tumor progression. *Biochimie* 2005;**87**:377–83.

62. Moller Sorensen N, Vejgaard Sorensen I, Ornbjerg Wurtz S *et al* Biology and potential clinical implications of tissue inhibitor of metalloproteinases-1 in colorectal cancer treatment. *Scand J Gastroenterol* 2008;**43**:774–86.